Proceedings of the 16th International IEEE Annual Conference on Intelligent Transportation Systems (ITSC 2013), The Hague, The Netherlands, October 6-9, 2013

GPS Multipath Detection and Rectification using 3D Maps

Shunsuke Miura[1], Shoma Hisaka[1] and Shunsuke Kamijo[1]

Abstract— **Global Navigation Satellite Systems (GNSSs) suffer from the problems of invisible satellites and multipath effect in urban canyons. Many approaches have been employed to eliminate multipath signals in order to reduce positioning errors. Among these, those that consider the geometry of surrounding buildings to improve the evaluation of possible multipath signals have gained most interest. However, such approaches, although successful, require many satellites for positioning after eliminating multipath signals. This study proposes an approach in which the multipath signals themselves are used for positioning error correction. The proposed algorithm evaluates the pseudoranges of the possible multipath signals by referring to the building geometry. The assumed position is estimated by using the pseudoranges and is evaluated by the likelihood of the possible positioning error. The proposed method was verified through field experiments in urban canyons in Tokyo.**

I. INTRODUCTION

For realizing Intelligent Transportation Systems (ITSs), one of the key requirements is reliably and accurately estimating the positions of road users such as vehicles and pedestrians. Now, in recent times, Global Positioning Systems (GPSs) have emerged as a suitable position estimation technology, and they have been widely incorporated into various daily-use devices such as vehicles and cellphones. Many types of advanced GPS receivers such as Differential GPS (D-GPS) and Real-Time Kinematic GPS, which can output precise positions by using ground-based reference stations, are currently available. Furthermore, in the near future, satellite navigation systems are expected to become more commonly available with the development of multiple Global Navigation Satellite Systems (GNSSs) such as the Chinese COMPASS system, European GALILEO system, and Japanese Quasi-Zenith Satellite System. A receiver equipped with an advanced antenna with a choke ring that can adapt to multiple frequencies and multiple GNSSs [1] can estimate its self-position very accurately. However, such advanced GPSs are not easily portable because they might require a relatively large antenna or a fast processing unit. Consequently, the GPS receivers commonly employed in vehicles and cellphones are low-cost single-frequency stand-alone modules. Under optimal conditions, these receivers provide the position with an accuracy of 10 m, which is adequate for rough navigation. However, the accuracy worsens in urban canyons with tall buildings because of the so-called multipath effect. The multipath effect is a propagation phenomenon that results from the reflection of electromagnetic waves from buildings or other surfaces. It may also be caused by diffraction from small objects such as traffic lights, road signs, and roadside trees. These effects may lead to a positioning error of more than 100 m in urban canyons [2]–[4]. To correctly estimate such errors by a stand-alone GPS receiver is not practical. Therefore, such receivers are not suitable for use in a positioning system from the viewpoint of road safety. For applications to collision avoidance systems, more accurate and reliable systems are essential.

Nonetheless, GPSs have found widespread use, and various improvements to them have been studied. Various hardware-based correlators that are more robust to the multipath effect have been developed [5]–[10], such as multipath-estimating delay-locked loop [9] and vision correlator [10]. Furthermore, various techniques have also been developed. The single-frequency precise point positioning technique was proposed to estimate a vehicle's position on motorways with a fine sky view [11]. GPS can, in conjunction with other sensors such as a camera or LIDAR, show improved positioning accuracy [12], [13]. GPS simulation systems for evaluating GPS multipaths in certain areas have also been developed [14], [15].

To improve the accuracy of GPS, many have suggested avoiding the use of Non-Line-of-Sight (NLOS) satellites for positioning. Accordingly, various multipath detection techniques have been proposed [12], [16]–[19]. Suzuki et al. [12] developed a system that integrated a GPS receiver with an omnidirectional far-infrared (IR) camera to capture the surrounding sky image to distinguish NLOS satellites. Peyret et al. [17] used digital maps to detect hidden satellites. Obst et al. [19] used a simple 3D ray-tracing method to estimate NLOS signals. In these systems, satellites that are estimated to be invisible are rejected in the positioning process.

This study aims to improve the position accuracy of an inexpensive GPS module by detecting multipath signals and correcting their measured pseudorange. This is realized by combining the searching algorithm, the 3D ray-tracing method, GPS positioning algorithm, particle filter, digital elevation model data, and 2D map data to distinguish NLOS satellites from among all the satellites observed by a receiver. By using this ray-tracing method, we propose an algorithm to accurately estimate positions in streets.

II. STRATEGY OVERVIEW

As mentioned above, various methods have been used to identify invisible satellites. However, all such methods require a large number of satellites because rejecting multipath signals decreases the number of satellites available for positioning. In urban areas consisting of many tall buildings, the number of visible satellites identified by these methods,

[1]Shunsuke Miura, Shoma Hisaka and Shunsuke Kamijo, are with Institute of Industrial Science, The University of Tokyo, 4-6-1 Komaba, Meguro-ku, Tokyo 153-8505 JAPAN, +81-3-5452-6273, kamijo@iis.u-tokyo.ac.jp

978-1-4799-2914-613/$31.00 ©2013 IEEE

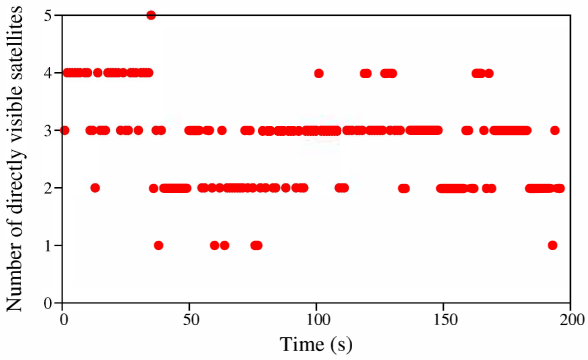

Fig. 1: Number of directly visible GPS satellites

which excludes the use of the pseudorange set from invisible satellites, often becomes less than four. However, a GPS receiver requires at least four satellites to calculate the position in three dimensions. If only three satellites are available, the GPS receiver outputs only 2D positions under the assumption that it is at mean sea level. Such 2D positioning could be hundreds of meters off depending on where the receiver really is. If less than three satellites are available, the receiver cannot calculate any positions.

Fig. 1 shows an example of the number of observed LOS GPS satellites at Hitotsubashi, Chiyoda-ku, Tokyo. Invisible satellites are excluded using a ray-tracing method. Clearly, only around a quarter of the time, more than four satellites are available. This shortage of satellites reduces the positioning accuracy and availability.

Worldwide, one trend has been to use multiple GNSSs, thus increasing the number of satellites, to estimate positions. However, we still consider it important to make optimal use of existing stand-alone single-frequency GPS devices. In this study, therefore, we focus on not reducing the number of measured satellites, and instead, we use their multipath signals themselves for positioning error correction.

III. SYSTEM SETUP

A. GPS Receiver

In our experiment, the receiver should be capable of outputting at least raw ephemeris data, GPS times, raw pseudorange set, and position outputs. To meet these criteria, we decided to use a u-blox NEO-6P GPS Evaluation Kit, a simple, small, low-cost, stand-alone, single-frequency GPS L1 receiver. It can output various types of GPS data such as raw pseudorange set for each satellite, stored ephemeris data, and calculated positions. Details about the output data provided by this receiver are listed in Table I.

B. 3D Ray-Tracing

Ray tracing is a technique that was originally used in the field of computer graphics to generate an image of objects by tracing the path of light. It is now also used to simulate radio propagation [20], [21].

The type of ray-tracing employed is called an image method. The surfaces of buildings are considered as perfectly

TABLE I: Details about output data provided by GPS receiver

Device name	u-blox NEO-6P GPS module
Antenna used	u-blox ANN-MS active GPS antenna with 5 m cable
Output data	Position, Velocity, DOP, Almanac, Ephemeris, GPS time, Satellite Status, GPS week, Pseudoranges, Signal strength C/No, etc.

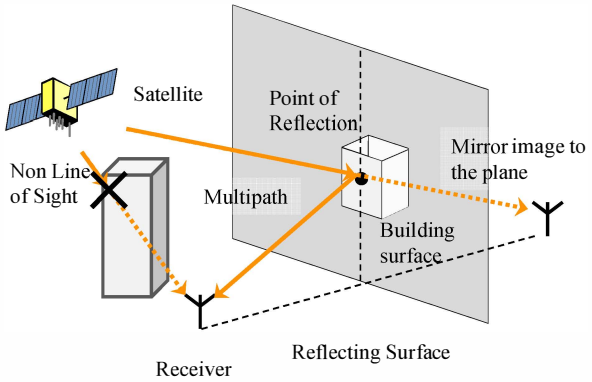

Fig. 2: Image method to find a reflected path.

Algorithm 1 Finding a reflected path

1: Compute the receiver's mirror image position to a building surface.
2: Prepare a line segment connecting the mirror image and a satellite.
3: Calculate an intersection of the line segment and a plane consisting of the building surface.
4: If the intersection is outside of the surface, a reflected path does not exist from the building.
5: If not, prepare two line segments connecting the point of reflection and the satellite, and the point of reflection and the receiver.
6: If both line segments are not blocked by some other structures, they are considered as a reflected path.

reflective smooth planes, i.e., as mirrors, and therefore, the rays obey the laws of reflection. The algorithm to find a reflected path is described in Algorithm 1 and illustrated in Fig. 2. Our GPS signal propagation simulation using 3D ray-tracing and 3D GIS data is shown in Fig. 3. Red lines denote the LOS path; green lines, the reflected paths; and blue lines, the NLOS paths. Our simulation can be used to distinguish reflected rays and to estimate the multipath error distance.

C. 3D Building Map

To create 3D building maps, we used building location data extracted from freely available 2D map data. Fig. 4 shows the process of creating a 3D building map. OpenStreetMap (OSM), a collaborative project that aims to create a freely editable map, provides 2D geographic information system (GIS) data about the layouts and positions of every object on the map, including roads and buildings. Moreover, OSM data can be easily edited to make the data more

978-1-4799-2914-613/$31.00 ©2013 IEEE

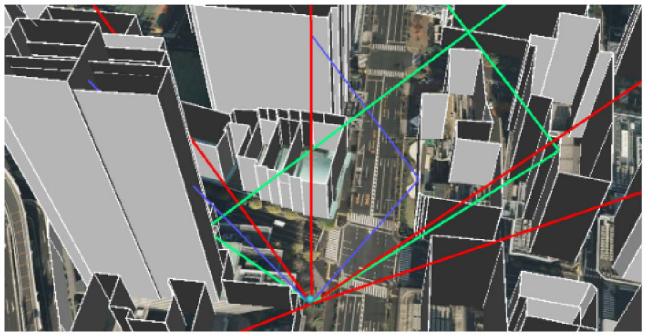

Fig. 3: Ray tracing simulation to calculate multipaths.

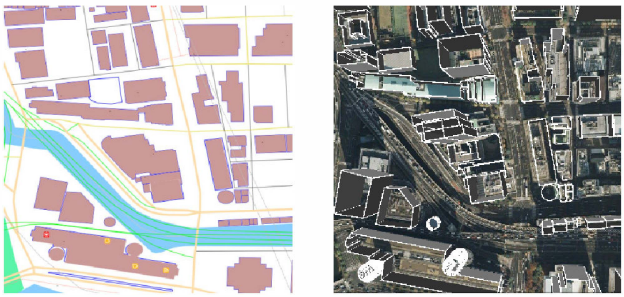

(a) 2D GIS data (b) 3D building map

Fig. 4: Creating 3D building map from 2D GIS data and 3D height data

accurate. Its building layouts are combined with good-3D, the 3D digital surface model (DSM) data provided by Aero Asahi Corporation, to generate 3D buildings maps. The good-3D DSM data has a horizontal resolution of 1 m and accuracy of 0.5 m and a vertical resolution of 0.01 m and accuracy of 0.15 m. Fig. 4(a) shows an example of 2D GIS data from OSM and Fig. 4(b), an example of 3D GIS data that we created.

We decided to create a 3D building map of the Hitotsubashi area. Tests were performed at a road intersection. The landscape of the road and the ray-tracing simulation are shown in Fig. 3. Because tall buildings are present on both sides of the road, we can see that 2-3 received signals are actually multipath signals.

D. Spatial Uncertainty of 3D Building Map

Because there is uncertainty in both the 3D DSM data and 2D GIS data, there must also be uncertainties in created 3D building map. This might lead wrong LOS/NLOS estimation. Thus, we must consider the possibility of multipath detection failure, especially in the situation that the signal ray pass through naer by buildings, or the ray is blocked at just nearby edges of building.

To suppress wrong multipath determination, the minimum distance to all surrounding buildings and the received signal strength are simply utilized in this for NLOS estimation. The minimum distance from the ray to buildings is calculated during the ray-tracing simulation. If the minimum distance $d_{\min}$ is less than a threshold distance $d_{\text{threshold}}$, the estimation is performed by referring to the received signal strength; the signal is considered as direct path if it is sufficiently strong compared to the average signal strength, whereas weak signals are considered as multipath. The threshold distance is determined based on the accuracy of the 3D building maps. NLOS detection result is made in accordance with the Table II.

TABLE II: Multipath estimation considering the uncertainty of 3D building map

Minimum distance	$d_{\min} > d_{\text{threshold}}$		$d_{\min} \leq d_{\text{threshold}}$	
Signal strength	strong	weak	strong	weak
LOS	Direct path		Direct path	Multipath
NLOS	Multipath		Direct path	Multipath

IV. PROPOSED ALGORITHM

The receiver output itself is not used as a reference position in this study because some unknown smoothing must be applied to it. In this section, first, the equations of GNSS positioning and the conventional method are explained. Secondly, the essence of a proposed positioning method is described. We introduce a new indicator in this section to search for the ground truth position based on the difference of calculated positions. The framework of tracking is discussed at the end of this section.

A. Weight Least Squares Solver

To obtain reference positioning data, we developed a conventional positioning method that uses raw pseudorange and raw ephemeris data measured using a GPS receiver. This method calculates the satellite positions according to the raw broadcast ephemeris and then estimates the 3D receiver position and receiver clock offset by using weighted least squares (WLS) estimation.

To determine the receiver position and receiver clock offset, pseudorange measurements are performed for at least four satellites. The relation between the pseudorange set, receiver positions, and satellite positions is written as

$$\boldsymbol{R} = \begin{bmatrix} R_1 \\ R_2 \\ \vdots \\ R_N \end{bmatrix} = \begin{bmatrix} \|\boldsymbol{x}_1^{\mathrm{sv}} - \boldsymbol{x}^{\mathrm{r}}\| + c\Delta t_1 \\ \|\boldsymbol{x}_2^{\mathrm{sv}} - \boldsymbol{x}^{\mathrm{r}}\| + c\Delta t_2 \\ \vdots \\ \|\boldsymbol{x}_N^{\mathrm{sv}} - \boldsymbol{x}^{\mathrm{r}}\| + c\Delta t_N \end{bmatrix} \quad (1)$$

where $\boldsymbol{R}$ denotes a vector of the measured pseudorange; n, the index of the satellite; N, the number of received satellite signals; R_n, the measured pseudorange for the n-th satellite; $\boldsymbol{x}_n^{\mathrm{sv}}$, the n-th satellite's position; $\boldsymbol{x}^{\mathrm{r}}$, the receiver position; $\|\boldsymbol{x}_n^{\mathrm{sv}} - \boldsymbol{x}^{\mathrm{r}}\| = \rho_n$, the geometric range between the n-th satellite and the receiver; c, the speed of light; and Δt, the error distance equivalent time. To solve (1) by the WLS method, N should be four or more.

Raw pseudorange data is simply derived by multiplying the signal propagation time and the speed of light. Because the signal propagation time includes numerous delays, such

as sources of final positioning errors, we have to correct the pseudorange. Each measured pseudorange R_n is written as

$$R_n = \rho_n + c(\delta t^{\mathrm{r}} - \delta t_n^{\mathrm{sv}}) + I_n + T_n + \varepsilon_n \qquad (2)$$

where δt_n^{sv} denotes the satellite clock offset time; δt^{r}, the receiver offset time; I, the ionospheric delay distance; T, the tropospheric delay distance; and ε, the errors caused by multipath propagation, receiver noise, and antenna delay.

In our positioning process, the satellite clock offset is corrected using values calculated from the broadcast ephemeris. The ionospheric delay correction obtained from the Klobuchar model and the tropospheric delay correction based on the Saastamoinen model are also applied. The remaining error is the multipath error and the receiver noise. Here, considering that noise is negligibly small, the only error to be removed is the multipath error to be estimated by the ray-tracing simulation.

Before we verify our proposed algorithm, we evaluate the conventional WLS method. We compared the data points computed by the receiver and our conventional method. Fig. 5 shows an overlay of its result on a map image. The blue triangles and red dots respectively represent points output by the receiver and points calculated by the conventional method. The white line indicates the true ground route that the receiver follows. This image suggests that the receiver outputs are somehow filtered to make the trajectory smooth. Because of this, the conventional method does not exactly fit the receiver outputs. Nonetheless, they have similar trends in error value and direction, and the differences are sufficiently small to consider our calculation as a conventional method.

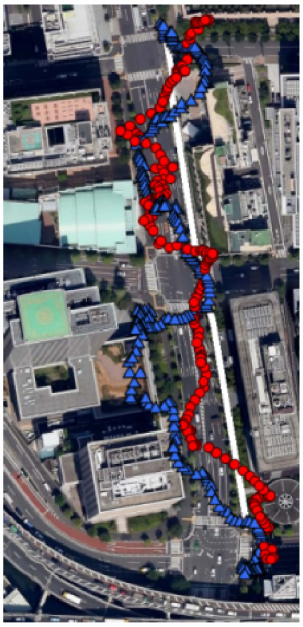

Fig. 5: Comparison between receiver outputs (blue triangles) and conventional method (red dots). The conventional method is calculated using the measured raw pseudorange set. The white line represents the true ground route.

B. Pseudorange Evaluation from Hypothesized Positions

By using the measured pseudorange set, 3D building map, ray-tracing, and WLS method, we propose a searching algorithm for accurately estimate positions. The concept is described below.

Every time the receiver outputs the measured pseudorange set $\boldsymbol{R} = [R_1, R_2, \cdots, R_N]^{\mathrm{T}}$, the position $\boldsymbol{y}_0$ is calculated by WLS using $\boldsymbol{R}$ and satellite positions $\boldsymbol{x}_n^{\mathrm{sv}} (n = 1, \cdots, N)$. The main idea used in this algorithm is to find reasonable positions $\boldsymbol{P}^{(i)}$, where i represents the index of samples, by searching around the reference position $\boldsymbol{y}_0$. Therefore, we sample some points $\boldsymbol{P}^{(i)}$ around $\boldsymbol{y}_0$, as illustrated in Fig. 6(a) Assuming $\boldsymbol{P}^{(i)}$ as hypothesized position of ground truth point, the possible multipath error distance $\varepsilon^{\mathrm{multipath}}$ from the point $\boldsymbol{P}^{(i)}$ to each satellite can be estimated by ray-tracing. Thus, we calculate a hypothesized pseudorange $\hat{R}_n^{(i)}$ from the point $\boldsymbol{P}^{(i)}$ to the n-th satellite $\boldsymbol{x}_n^{\mathrm{sv}}$ as a sum of the geometric distance $\rho_n^{(i)} = \|\boldsymbol{x}_n^{\mathrm{sv}} - \boldsymbol{P}^{(i)}\|$, satellite clock offset distance $c\delta t_n^{\mathrm{sv}}$, receiver clock offset $c\delta t^{\mathrm{r}}$, ionospheric delay distance I_n, tropospheric delay distance T_n, and multipath error distance $\varepsilon_n^{\mathrm{multipath(i)}}$.

$$\begin{aligned}\hat{\boldsymbol{R}}^{(i)} &= \left[\hat{R}_1^{(i)}\ \hat{R}_2^{(i)}\ \cdots\ \hat{R}_N^{(i)}\right]^{\mathrm{T}} \\ &= \boldsymbol{\rho}^{(i)} + c(\boldsymbol{\delta t}^{\mathrm{r}} - \boldsymbol{\delta t}^{\mathrm{sv}}) + \boldsymbol{I} + \boldsymbol{T} + \boldsymbol{\varepsilon}^{\mathrm{multipath}(i)} \end{aligned} \qquad (3)$$

Because each term is calculated separately, this hypothesized pseudorange set is not dependent on the measured pseudorange set $\boldsymbol{R}$ at all. By using this set $\hat{\boldsymbol{R}}^{(i)}$, a position $\hat{\boldsymbol{y}}^{(i)}$ is calculated by WLS. Here, it should be noted that this hypothesized pseudorange $\hat{R}_n{}^{(i)}$ potentially contains a multipath error distance. Thus, some of the calculated position $\hat{\boldsymbol{y}}^{(i)}$ might appear close to point $\boldsymbol{P}^{(i)}$ and some might be far from point $\boldsymbol{P}^{(i)}$. Fig. 6(b) shows two sampling points illustrated in Fig. 6(a) along with the corresponding calculated positions $\hat{\boldsymbol{y}}^{(i)}$; $\hat{\boldsymbol{y}}^{(1)}$ actually appears very close to $\boldsymbol{P}^{(1)}$, whereas $\hat{\boldsymbol{y}}^{(2)}$ appears far from $\boldsymbol{P}^{(2)}$. However, we realize that the calculated position $\hat{\boldsymbol{y}}^{(i)}$ must appear around $\boldsymbol{y}_0$ if the hypothesized pseudorange set $\hat{\boldsymbol{R}}^{(i)}$ is affected by the multipath in the same way as the measured pseudorange set is. Accordingly, we assume that point $\boldsymbol{P}^{(i)}$ is where the receiver actually is if the distance between $\hat{\boldsymbol{y}}^{(i)}$ and $\boldsymbol{y}_0$ is sufficiently small. Therefore, we propose using the distance $\|\boldsymbol{y}_0 - \hat{\boldsymbol{y}}^{(i)}\|$ as an indicator of the likelihood value for each hypothesis $\boldsymbol{P}^{(i)}$. The calculated positions $\hat{\boldsymbol{y}}^{(i)}$ for every sampling point $\boldsymbol{P}^{(i)}$, presented in Fig. 6(a), are illustrated in Fig. 6(c).

Considering these calculations, we need to evaluate the condition of sampling points $\boldsymbol{P}^{(i)}$. $\boldsymbol{P}^{(i)}$ can be one of the reasonable positions if $\boldsymbol{P}^{(i)}$ satisfies

- $\boldsymbol{P}^{(i)}$ should be outside any building if any signal strength is sufficiently strong,
- $\boldsymbol{P}^{(i)}$ should be directly visible from satellites whose signal strength is sufficiently strong compared to the average signal strength,
- $\boldsymbol{P}^{(i)}$ should be NLOS whose signal strength is sufficiently weak compared to the average signal strength,

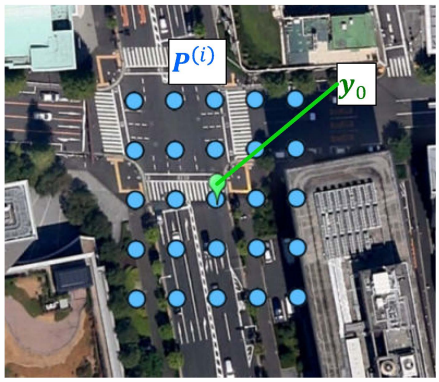

(a) Examples of reference position $\boldsymbol{y}_0$ and sampling points $\boldsymbol{P}^{(i)}$

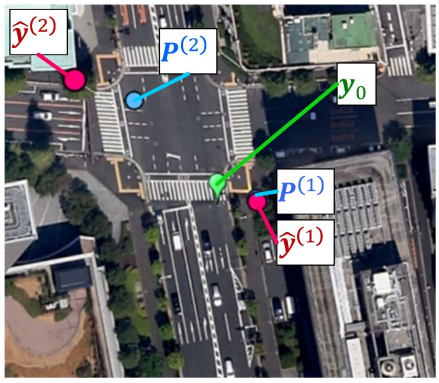

(b) Examples of calculated positions $\hat{\boldsymbol{y}}^{(1)}$, $\hat{\boldsymbol{y}}^{(2)}$, sampling points $\boldsymbol{P}^{(1)}$, $\boldsymbol{P}^{(2)}$ and reference position $\boldsymbol{y}_0$

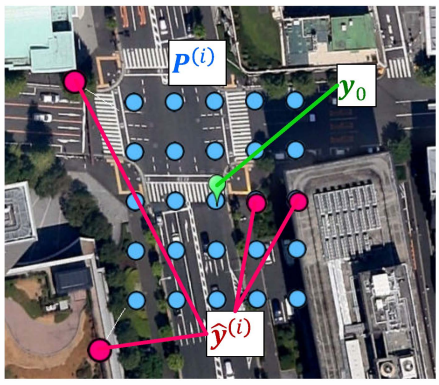

(c) Examples of every calculated position $\hat{\boldsymbol{y}}^{(i)}$ for $\boldsymbol{P}^{(i)}$ overlaid on (a)

Fig. 6: Sampling around reference position $\boldsymbol{y}_0$ and evaluation process

$\hat{\boldsymbol{y}}^{(i)}$ is calculated for all $\boldsymbol{P}^{(i)}$ that satisfies above requirements.

C. Position Estimation by Grid Search

For the estimation and tracking of the receiver positions, we prepared grids to sample points. Two types of grids are utilized in this study as shown in Fig. 7; one covers a 50-m × 50-m area with 5-m intervals and the other one covers a 5-m × 5-m area with 0.5-m intervals. Let the points on the large grid be represented by $\boldsymbol{P}^{(i)}$ and those on the small grid, by $\boldsymbol{P}^{(j)}$. By using the proposed evaluation method, considering each grid point as a hypothesized position $\boldsymbol{P}^{(i)}$, the confidences $w^{(i)}$ of the points on the grids are calculated by the following formula.

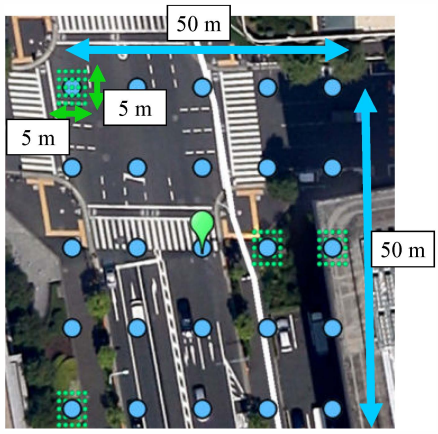

Fig. 7: Example of two types of grids for sampling points. Large blue circles represent large grids,; and small green circles, small grids.

$$w^{(i)} = \begin{cases} \frac{1}{\|\boldsymbol{y}_\bullet - \hat{\boldsymbol{y}}^{(i)}\|} & (\|\boldsymbol{y}_0 - \hat{\boldsymbol{y}}^{(i)}\| < k_{\text{threshold}}) \\ 0 & (otherwise) \end{cases} \tag{4}$$

The receiver position $\boldsymbol{x}^{\text{r}}$ is calculated by

$$\boldsymbol{x}^{\text{r}} = \frac{\sum_i w^{(i)} \boldsymbol{P}^{(i)}}{\sum_j w^{(i)}} \tag{5}$$

This algorithm is summarized in detail as algorithm 2 and an example of sampling grids is illustrated in Fig. 7.

Algorithm 2 Position Estimation Algorithm

1: Every time the receiver outputs raw pseudorange set, calculate position $\boldsymbol{y}_0$ by WLS using $\boldsymbol{R} = [R_1\ R_2\ \cdots\ R_N]^{\text{T}}$
2: Divide a 50 m × 50 m area around $\boldsymbol{y}_0$ into 5 × 5 grids
3: **for all** i for the points on the large grid $\boldsymbol{P}^{(i)}$ **do**
4: Set $\hat{\boldsymbol{R}}^{(i)} \leftarrow \boldsymbol{\rho}^{(i)} + c(\boldsymbol{\delta t}^{\text{r}} - \boldsymbol{\delta t}^{\text{sv}}) + \boldsymbol{I} + \boldsymbol{T} + \varepsilon^{\text{multipath}(i)}$
5: Calculate $\hat{\boldsymbol{y}}^{(i)}$ by WLS using $\hat{\boldsymbol{R}}^{(i)}$
6: **if** $\|\boldsymbol{y}_0 - \hat{\boldsymbol{y}}^{(i)}\| < k_{\text{threshold}}$ **then**
7: divide a 5 m × 5 m area around $\boldsymbol{P}^{(i)}$ into 5 × 5 grids
8: **for all** j for the points on the small grid $\boldsymbol{P}^{(j)}$ **do**
9: Set $\hat{\boldsymbol{R}}^{(j)} \leftarrow \boldsymbol{\rho}^{(j)} + c(\boldsymbol{\delta t}^{\text{r}} - \boldsymbol{\delta t}^{\text{sv}}) + \boldsymbol{I} + \boldsymbol{T} + \varepsilon^{\text{multipath}(j)}$
10: Calculate $\hat{\boldsymbol{y}}^{(j)}$ by WLS using $\hat{\boldsymbol{R}}^{(j)}$
11: Calculate the weight $w^{(j)}$ by (4)
12: **end for**
13: **end if**
14: **end for**
15: Calculate weighted average position $\tilde{\boldsymbol{x}}^{\text{r}}$
$\tilde{\boldsymbol{x}}^{\text{r}} \leftarrow \left[\sum_j \frac{\sum_i w^{(i)} \boldsymbol{P}^{(i)}}{\sum_j w^{(i)}}\right.$
16: Output $\tilde{\boldsymbol{x}}^{\text{r}}$ as an estimated position.

978-1-4799-2914-613/$31.00 ©2013 IEEE

D. Smoothing by Particle Filter

Because the receiver outputs are somehow filtered and smoothened, we decided to apply a filter for our conventional method and proposed method to smoothen the trajectories of the estimated positions. A particle filter that can estimate the states of nonlinear systems with non-Gaussian noise is employed for this purpose.

To use the particle filter, we need to design the state dynamics model, state vector, and likelihood function that give weight to each particle. The observation vector is $\boldsymbol{z}_t = [\varphi^{\mathrm{GPS}}, \lambda^{\mathrm{GPS}}]^{\mathrm{T}}$, a two-dimensional coordinate position estimated above. The state vector is defined as $\boldsymbol{x}_t = [\varphi, \lambda, v_\varphi, v_\lambda]^{\mathrm{T}}$, where φ and λ respectively denote the latitude and longitude with corresponding velocities v_φ and v_λ. Considering the noise $\boldsymbol{N}_t \sim \mathcal{N}(\boldsymbol{0}, \sigma^2)$, its motion is expressed as follows:

$$\boldsymbol{x_t} = F\boldsymbol{x}_{t-1} + \boldsymbol{N}_t \tag{6}$$

$$F = \begin{bmatrix} 1 & 0 & \Delta t & 0 \\ 0 & 1 & 0 & \Delta t \\ 0 & 0 & 1 & 0 \\ 0 & 0 & 0 & 1 \end{bmatrix} \tag{7}$$

This filter is performed with a set of particle samples $\boldsymbol{P}_t = \left\{\boldsymbol{p}_t^{(1)}, \boldsymbol{p}_t^{(2)}, \cdots, \boldsymbol{p}_t^{(N_p)}\right\}$. The volume of the particles is 2,000 in this study. In filter updating process, the likelihood $\alpha_t^{(i)}$ for each sample $\boldsymbol{p}_t^{(i)} = [\varphi^{(i)}, \lambda^{(i)}, v_\varphi^{(i)}, v_\lambda^{(i)}]^{\mathrm{T}}$ is determined every second by a likelihood function (8):

$$\begin{aligned} \alpha_t^{(i)} &= L\left(\boldsymbol{z_t} | \boldsymbol{x_t} = \boldsymbol{p}_{t|t-1}^{(i)}\right) \\ &= \left[\left(\varphi^{\mathrm{GPS}} - \varphi^{(i)}\right)^2 - \left(\lambda^{\mathrm{GPS}} - \lambda^{(i)}\right)^2\right]^{-1/2} \end{aligned} \tag{8}$$

V. EXPERIMENTAL RESULT

Field tests were conducted in January 2013 at the Hitotsubashi intersection mentioned in section 3.2. During the tests, all receiver outputs were obtained at a rate of 1 Hz.

Fig. 8 shows the trajectories of the conventional and the proposed method. As mentioned before, we used a particle filter to make the output smoother. The red dots and yellow squares on the map respectively represent the result of the conventional and the proposed method. Fig. 8(a) shows the estimated points by the proposed method without considering the uncertainty of 3D building map and Fig. 8(b), with considering the uncertainty of 3D building map.

In this case, a receiver moved along a sidewalk from the lower right of the picture to the top middle. This route is approximately 250 m and takes about 180 seconds to walk. For a quantitative evaluation, we considered the error distance as the minimum distance from the true ground line to each estimated position. In Table III, the maximum, the mean and the sample variance of error distances for a test without and with considering the uncertainty of 3D building map are shown. Fig. 9 draws an example of the errors through one test. This result shows that by using the proposed algorithm, the maximum error can be reduced from 33.0 to 9.0 m and the average error can be reduced from 12.0 to 3.4 m, According to Fig. 8 and Table III, the errors of some points become smaller by simply considering the uncertainty

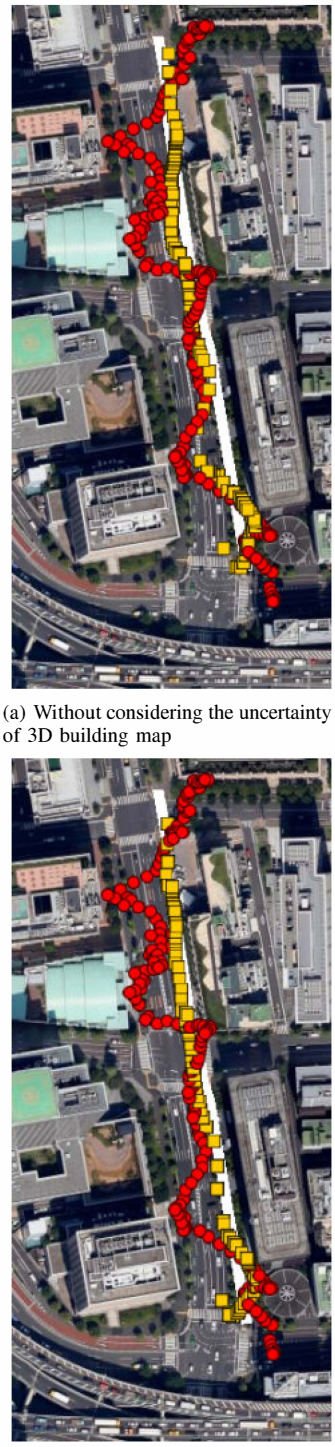

(a) Without considering the uncertainty of 3D building map

(b) With considering the uncertainty of 3D building map

Fig. 8: Comparison of trajectories between conventional method (red dots) and proposed method (yellow squares). White line indicates the true route.

978-1-4799-2914-613/$31.00 ©2013 IEEE

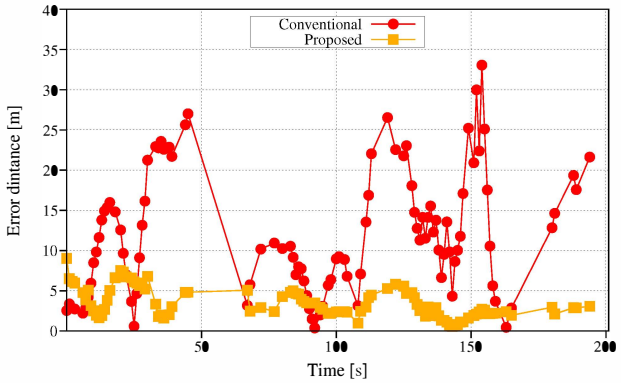

Fig. 9: Comparison of error distance between the conventional method (red dots) and the proposed method (yellow squares)

TABLE III: Maximum, mean and standard deviation of error

Case	Maximum Error [m]	Mean Error [m]	Standard deviation [m]
Conventional	33.0	12.0	7.5
Proposed (without map uncertainty)	13.5	3.6	2.5
Proposed (with map uncertainty)	9.0	3.4	1.8

of 3D building map.

VI. CONCLUSIONS

We have proposed an algorithm that uses 3D building map and a ray-tracing method to improve the accuracy of mobile GPS devices. By using our ray-tracing simulation with considering the uncertainty of 3D building map, invisible satellites can be effectively identified and the potential multipath error distance can be estimated. By calculating the pseudorange set from a position considering corrections including multipath error correction, we can estimate the position calculated using this pseudorange set by WLS estimation. If the distance between the positions calculated using the estimated and the measured pseudorange set is less, we can assume that the position is where the receiver actually is.

This supposition was evaluated through field experiments, and it was found to greatly improve the positioning accuracy. The result shows that the error distances are within 10 m at most points in the proposed method. However, some points still deviate from the true ground path. In addition to these points, the availability of the positioning was decreased compared to the conventional method because of the existence of multiple reflected signals and diffracted signals that cannot simulated by our current ray-tracing method. We will investigate these remaining errors in future work. Furthermore, we will conduct tests in other areas with different building geometries.

REFERENCES

[1] JK Ray, ME Cannon, and P. Fenton. GPS code and carrier multipath mitigation using a multiantenna system. *Aerospace and Electronic Systems, IEEE Transactions on*, Vol. 37, No. 1, pp. 183–195, 2001.

[2] G. MacGougan, G. Lachapelle, R. Klukas, K. Siu, L. Garin, J. Shewfelt, and G. Cox. Performance analysis of a stand-alone high-sensitivity receiver. *GPS Solutions*, Vol. 6, No. 3, pp. 179–195, 2002.

[3] O Mezentsev, Y Lu, G Lachapelle, and R Klukas. Vehicular navigation in urban canyons using a high sensitivity GPS receiver augmented with a low cost rate gyro. In *Institute of Navigation GPS Conference*, Vol. 15, pp. 263–369, 2002.

[4] J.H. Wang and Y. Gao. High-sensitivity GPS data classification based on signal degradation conditions. *Vehicular Technology, IEEE Transactions on*, Vol. 56, No. 2, pp. 566–574, 2007.

[5] L. Garin and J.M. Rousseau. Enhanced strobe correlator multipath rejection for code & carrier. In *Proceedings of the 10th International Technical Meeting of the Satellite Division of The Institute of Navigation (ION GPS 1997)*, pp. 559–568, 1997.

[6] AJ Van Dierendonck, P. Fenton, and T. Ford. Theory and performance of narrow correlator spacing in a GPS receiver. *Navigation*, Vol. 39, No. 3, pp. 265–283, 1992.

[7] B. Townsend and P. Fenton. A practical approach to the reduction of pseudorange multipath errors in a L1 GPS receiver. In *Proceedings of the 7th International Technical Meeting of the Satellite Division of the Institute of Navigation, Salt Lake City, UT, USA*, 1994.

[8] M.S. Braasch. Performance comparison of multipath mitigating receiver architectures. In *Aerospace Conference, 2001, IEEE Proceedings.*, Vol. 3, pp. 3/1309 –3/1315 vol.3, 2001.

[9] B.R. Townsend, P.C. Fenton, KJ Van Dierendonck, and D.J.R. Van Nee. Performance evaluation of the multipath estimating delay lock loop. *NAVIGATION-LOS ANGELES AND WASHINGTON-*, Vol. 42, pp. 503–514, 1995.

[10] P.C. Fenton and J. Jones. The Theory and Performance of NovAtel Inc. ' s Vision Correlator. *ION GNSS*, 2005.

[11] V.L. Knoop, P.J. Buist, C.C.J.M. Tiberius, and B. van Arem. Automated lane identification using precise point positioning an affordable and accurate GPS technique. *15th International IEEE Annual Conference on Intelligent Transportation Systems*, 2012.

[12] T. Suzuki, M. Kitamura, Y. Amano, and T. Hashizume. High-accuracy GPS and GLONASS positioning by multipath mitigation using omnidirectional infrared camera. In *Robotics and Automation (ICRA), 2011 IEEE International Conference on*, pp. 311 –316, may 2011.

[13] Yoshiko KOJIMA, Noriyoshi SUZUKI, Eiji TERAMOTO, and Hiroshi MURASE. Proposal of Precise Positioning Method Based on Accumulated GPS Raw Data : Basic study for a moving vehicle. *IEICE technical report*, Vol. 110, No. 150, pp. 1–6, 2010. (in Japanese).

[14] YongCheol SUH and Ryosuke SHIBASAKI. Evaluation of Satellite-Based Navigation Services in Complex Urban Environments Using a Three-Dimensional GIS. *IEICE transactions on communications*, Vol. 90, No. 7, pp. 1816–1825, jul 2007.

[15] J. Marais, M. Berbineau, and M. Heddebaut. Land mobile GNSS availability and multipath evaluation tool. *Vehicular Technology, IEEE Transactions on*, Vol. 54, No. 5, pp. 1697 – 1704, sept. 2005.

[16] Tatsuya Iwase, Noriyoshi Suzuki, and Yusuke Watanabe. Estimation and exclusion of multipath range error for robust positioning. *GPS solutions*, Vol. 17, No. 1, pp. 53–62, 2013.

[17] Franois Peyret, David Btaille, Miguel Ortiz, Stephan Miquel, and Leila Fontenay. How to improve GNSS positioning quality of service for demanding ITS in city environments by using 3D digital maps. In *19th ITS World Congress, Vienna, Austria, 22-26 October*, 2012.

[18] R. Shibazaki N. Kubo, A. Yasuda. An effective multipath mitigation technique under strong multipath environments. *The 2005 International Symposium on GPS/GNSS*, 8-10 December 2005.

[19] M. Obst, S. Bauer, P. Reisdorf, and G. Wanielik. Multipath detection with 3D digital maps for robust multi-constellation GNSS/INS vehicle localization in urban areas. In *Intelligent Vehicles Symposium (IV), 2012 IEEE*, pp. 184 –190, june 2012.

[20] Henry L Bertoni. *Radio propagation for modern wireless systems*. Pearson Education, 1999.

[21] Magdy F Iskander and Zhengqing Yun. Propagation prediction models for wireless communication systems. *Microwave Theory and Techniques, IEEE Transactions on*, Vol. 50, No. 3, pp. 662–673, 2002.